PV Grid Inverter Dynamics on Load Active and Reactive Power Demand for Weak Grid Stability

Shaka Kargbo
Electrical Engineering Department
Diponegoro University
Semarang, Indonesia
shakakargbo@students.undip.ac.id

Hermawan
Electrical Engineering Department
Diponegoro University
Semarang, Indonesia
hermawan@lecturer.undip.ac.id

Susatyo Handoko
Electrical Engineering Department
Diponegoro University
Semarang, Indonesia
susatyo@elektro.undip.ac.id

Iwan Setiawan
Electrical Engineering Department
Diponegoro University
Semarang, Indonesia
iwansetiawan@live.undip.ac.id

Trias Andromeda
Electrical Engineering Department
Diponegoro University
Semarang, Indonesia
triasandromeda@lecturer.undip.ac.id

***Abstract* — Energizing inductive loads on a weak grid network requires extra reactive power compensation such as STATCOM, capacitor bank, Grid-connected inverter system etc. The optimization of photovoltaic grid-connected power systems has limited the reactive power compensation to the inverter's capacity and consideration of its life cycle. In balancing the two limitations, oversizing the inverter can enable reactive power injection with a long-living operation. However, allowing excessive reactive power flow can also affect the active power requirement of the inductive loads. In this paper, a three-phase Grid-connected PV inverter simulation is made to investigate the inverter's and load's behavior when injecting reactive power required by the load to maintain a sufficient voltage on the grid. The inverter was oversized to a 1.60 AC-DC ratio. The system is simulated on the day and night motor startup operation with a 5ph induction motor started on the direct online method. The simulation results show that the motor power absorption is deficient when high reactive power is compensated.**

Keywords— PV Grid inverter dynamics, active and reactive power, induction motor, Direct Online, and weak grid stability.

I. INTRODUCTION

The need for PV reactive power on weak grids has rapidly captured researchers' attention for cost reduction considering the losses and the inverter durability [1]. The photovoltaic (PV) panel is primarily injecting active power into the grid. In contrast, the reactive power injection is based on the application's demand, such as dynamic application for grid stability on instantaneous disturbances and static application for conserving a constant grid voltage level [2]. Among the several power quality disturbances that require dynamic reactive power application, Induction Motor (IM) counts a lot on the weak grid during startup. The starting current is 5 to 8 times higher than the full-load current for the direct online (DOL) method, which can cause voltage dip beyond the tolerable limits specified by IEEE Std 1959-1995. In addition, it can adversely affect the operation of other loads connected to the grid [3], which triggered the need for reactive power [4], [5]. IMs are the highest power-consuming motors in the industry [6]. However, they are the favorite motors used for their numerous advantages [7].

The reactive power is needed in good quantity to control the grid voltage levels. It is widely agreed as the solution for weak grid stability. However, studies have proved that reactive power has a noticeable effect on the grid's performance [8], affecting the active power. As a result, minimizing the amount of reactive power in the network is a good practice. Excessive reactive power in the system can result in unwanted voltage drops and losses. When requested by the IM startup, a good step of supplying reactive power is by oversizing the inverter, as stated in literature [9]. It can ensure effectiveness in the grid PV inverter's reactive power supply during IM startup. Typically, oversizing inverters can increase operating costs. However, optimal oversizing such as between 10% to 60% [10], can resolve both cost and stability issues. The inverter's appropriate sizing can be used on both Day Mode Operation (DMO) and night mode Operation (NMO). Thus, the inverters can provide sufficient reactive power for IM startup [11], [9]. M. Habyarimana et al. [12] gave a descriptive analysis of the four IM startup methods and compensated reactive power on starting 5hp IM DOL using a capacitor bank.

Specifying reactive power requirements by IM makes the compensation easier for fast reactive power applications. Pichai Aree [7] gave the active and reactive power requirement for small and large IMs, while Ding Wang et al. [13] balanced the IM's active and reactive powers based on the Q-V plane operating points. IM's effect affects the grid in different parts such as the grid point of common contact (PCC), transmission substations etc. [14].

This paper investigates the PV inverter and IM behavior when compensated high motor required reactive power. The simulation provides active and reactive power required by the motor to manage the grid voltage to an appropriate level. The inverter used was oversized to 60% for this purpose. The system is simulated by Power simulation (PSIM) software on DMO and NMO with a 5hp IM started on the DOL method.

II. CONTROL METHOD OF THE SYSTEM

The three-phase PV grid-connected system topology in Fig. 1 composed of a grid system and a PV array with a two-stage converter coupling LCL filter to the grid [15][16] with transformerless synchronization to minimize the losses, the cost of the transformer, and the complexity of controlling the grid current of the inverter [17]. The PV array consists of PV panels arranged in a series-parallel configuration with the optimum number to provide the grid-connected PV specified power. The generated voltage from the PV is stepped up via the boost converter on the first stage of the double-stage conversion using incremental and conductance (INC) maximum power point tracker (MPPT). The inverter's output through the LCL filter is synchronized with the grid using a Dual Second Order Generalized Integrator-based Phase-locked Loop control (DSOGI-PLL). The entire PV topology

This research is funded by the Government of Indonesia h

is integrated with a weak grid network whose impedance short-circuit ratio is less than 10, and its reactance-resistance ratio is less than 0.5. The weak grid-connected PV system is loaded with DOL IM.

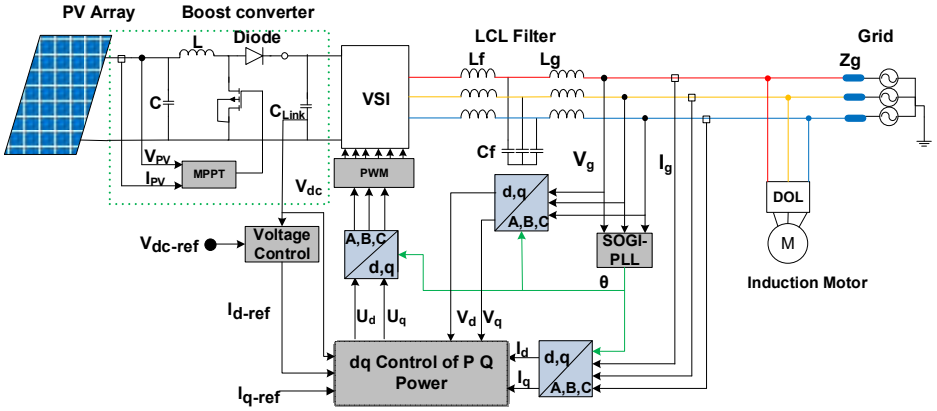

Fig. 1: PV Grid-Connected System Block Diagram

The system controlled the active and reactive power from the PV array. In delivering the PV active power to the grid, the MPPT implemented on the DC-DC converter tracked the PV's maximum power and transmitted it to the voltage source inverter (VSI) [18]. All the controls in the designed system, such as MMPT control, synchronization control, voltage control, and inverter inner current control, used the Proportional-integral (PI) controller, as stated by Setiawan Iwan et al. [19], tracking the reference signals for generating the required controlled signals. In addition, the park transformation is used in converting the voltages and currents from ABC to DQ frame and vice vasa [20].

A. Voltage Synchronization

Grid synchronization used the phase-locked-loop (PLL) concept to track the grid voltage frequency and phase for synchronizing the inverter current. The DSOGI-PLL based on the synchronous reference frame (SFR) with a filter as a modification is implemented in this study to estimate the phase and frequency of the grid voltage [20]. The grid voltages in the ABC frame, as shown in Fig. 1 above, are converted to αβ Stationary Frame via Clarke Transformation for the DSOGI input signal. The DSOI shifted the αβ signals by 90°and extracts its Positive Sequence for the SRF-PLL input. The αβ frame is converted to the DQ frame, and then the PI controller in the PLL estimates the frequency and phase angle by setting the q-axis voltage to zero. The estimated phase and frequency of the grid voltage are used in the Park transformation to generate the DQ signals used in the controls and the ABC voltage signal of the PWM.

B. Active power model

The DC-Link voltage control is the external active power control used to deliver the PV maximum power via the converters to the grid. The simple topology shown in Fig. 2 (a) is the actual block of the simulation. The PI controller regulates the DC-link capacitor voltage using a dc reference voltage to generate the d-axis reference current for the inverter's active power injection to the grid. Assuming that the inverter loss is minimal and negligible, the inverter output active power (P_{AC}) injected to the grid equals the PV maximum power (P_{PV}) in (1) the solar array produced. Thus, V_{DC}, I_{DC}, V_{gm}, and I_{gd} are the DC voltage and current, grid peak phase voltage, and the d-axis current.

$$P_{PV}=V_{DC}I_{DC}\cong P_{AC}=\frac{3}{2}V_{gm}I_{gd} \quad (1)$$

The voltage control gain is determined from (1) by considering the DC converter's mean current I_{DC} to the inverter and the d-axis reference current $I_{d\text{-}ref}$. With the assumption that the d-axis reference current $I_{d\text{-}ref}$ equals the grid reference current, and losses are negligible [21], the DC-Link gain as seen from the simplified model in Fig. 2(b) can be deduced to (2).

$$G=\frac{I_{DC}^{mean}}{I_{d\text{-}ref}}=\frac{3}{2}\frac{V_{gm}}{V_{DC\text{-}ref}} \quad (2)$$

When the current absorbed by the load I_L is zero, the DC voltage control gain shown in Fig. 2(c) is deduced to (3), where the current to the inverter I_{DC} equals the current flows to the capacitor I_C.

$$G_{dc}=\frac{V_{DC}}{V_{DC\text{-}ref}}=\frac{3}{2}\frac{V_{gm}}{V_{DC\text{-}ref}}\cdot\frac{1}{Cs} \quad (3)$$

C. Reactive Power Model

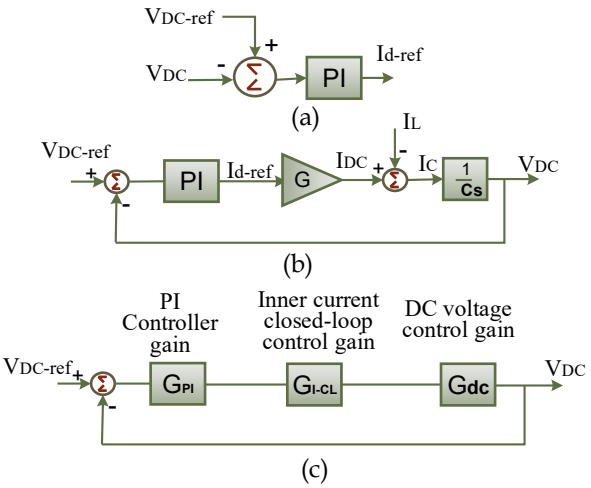

Fig. 2: (a) DC-Link PI control block (b) modified voltage control (c) voltage closed-loop control

The q-axis reference current used by the VSI internal control for reactive power injection is the external reactive power control output from the IM absorbed power. At grid synchronization, the voltage PI controller accurately controlled the d-axis reference current for the inverter's output active AC power to equal the input DC power by setting the q-axis reference current to zero. When initializing IM on the grid, the reactive power absorbed by the IM is taking as the inverter's reference reactive power. The IM absorbed powers in (4) as the reference powers for the simulation are generated on the DQ reference frame as given by [19].

$$P_{ref}=\frac{3}{2}V_{gd}\,I_d\,,\qquad Q_{ref}=\frac{3}{2}V_{gd}\,I_q \tag{4}$$

The reference q-axis current for the inner current controller is derived from the reference powers and grid voltage (5) [4].

$$I_{q\text{-}ref}=\frac{2}{3}\left(\frac{1}{V_{gd}^2+V_{gq}^2}\right)\left(P_{ref}V_{gq}-Q_{ref}V_{gd}\right) \tag{5}$$

D. Inverter Current Control

The inverter current control is the overall internal control loop of the active and reactive power of the inverter. The internal and external control loops are cascaded since the internal control uses the external controls' output, i.e., the DC voltage control output for active power and the load absorbed current for reactive power. Since the converters can add harmonic impurities into the current, the filter is used in controlling the grid current.

The filter gain in (6) used by the controller is derived from the filter's inductances (L_f and L_g), capacitance C_f and resistance R_f components by implementing s-domain analysis [22]. Furthermore, a series resistor is added to the capacitor as a damping factor to stabilize the control, as showed in Fig. 3. The complete topology of the filter interfacing the inverter and the grid is shown in Fig. 1.

$$G_f=\frac{I_{g(S)}}{V_{i(S)}}=\frac{C_fR_fS+1}{C_fL_fL_gS^3+C_fR_f(L_f+L_g)S^2+(L_f+L_g)S} \tag{6}$$

The current control uses a PI controller for this design to control the active and reactive current by feeding the grid current as a reference signal and cross-coupling the voltage to give the pulse width modulation (PWM) input voltage signals, as shown in Fig. 4(a). By applying Kirchhoff's laws to Fig.3, the inverter output is expressed as;

$$\begin{cases} L_f\dfrac{di_{ni}}{dt}=v_{ni}-v_{nx} \\ c_f\dfrac{dv_{nx}}{dt}=i_{ni}-i_{ng} \\ L_g\dfrac{di_{ng}}{dt}=v_{nx}-v_{ng} \end{cases} \tag{7}$$

Where n is the ABC frame, v_{ni}, $v_{n\text{-}x}$ and v_{ng} are the inverter, node, and grid voltages, respectively. i_{ni}, i_{nf} and i_{ng} are the inverter, capacitor branch, and grid currents, respectively. The resonant frequency of the filter should maintain the condition $10 < f_{res} < \frac{1}{2}f_{sw}$. Where f_{sw} is the switching frequency, and f_{res} is the resonant frequency. At the lower frequency range, the LCL acts as an inductor [23]. Hence the inverter output current be modeled by neglecting the filter's capacitor and summing the inductors ($L=L_f+L_g$) with the inverter current equals the grid current, then (7) can be written as,

$$L\frac{di_{ng}}{dt}=v_{ni}-v_{ng} \tag{8}$$

The grid voltage and current in the ABC frame of (8) are converted into the DQ frame using park transformation as;

$$\begin{cases} L\dfrac{di_{dg}}{dt}=v_{di}+\omega Li_{qg}-v_{dg} \\ L\dfrac{di_{qg}}{dt}=v_{qi}-\omega Li_{dg}-v_{qg} \end{cases} \tag{9}$$

The dynamics of the inverter currents on the DQ-frame shown in (9) consist of cross-coupled components, making the equation nonlinear. To decouple and linearize the dynamic inverter equation, (10) is developed, and it is represented in the control topology shown in Fig. 4(a) [23].

$$\begin{cases} u_{di}=v_{di}+\omega Li_{qg}-v_{dg} \\ u_{qi}=v_{qi}-\omega Li_{dg}-v_{qg} \end{cases} \tag{10}$$

The closed-loop control of the inverter current showed in Fig. 4(b) is comprised of three gains; the PI controller gain in (12), the PWM gain, which is obtained from the dc voltage and switching delay, as given in (11), and the LCL filter gain in (6).

$$G_{PWM}=\frac{V_{dc}}{2}\left(\frac{1}{1+sT_{sw}}\right) \tag{11}$$

$$G_{PI}=\frac{K_P\,S+K_I}{S}=k_p\left(1+\frac{1}{s\tau_i}\right) \tag{12}$$

K_p & K_i are the PI gains, $\tau_i = {}^{K_p}/_{K_i}$ is the time constant, T_{sw} is the switching time.

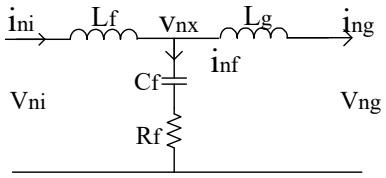

Fig. 3: Grid Inverter LCL filter design

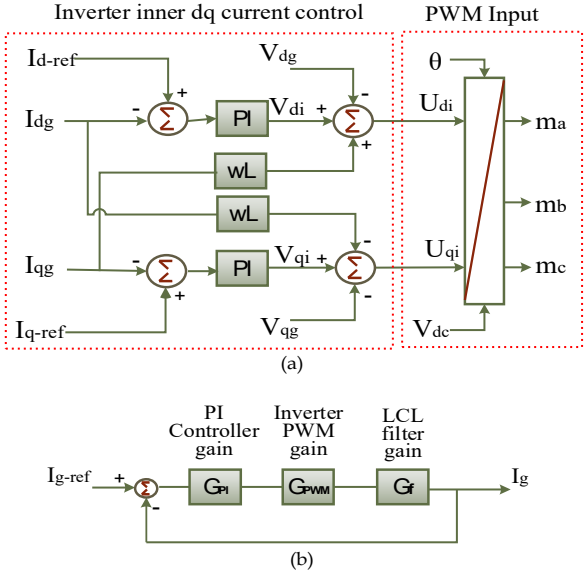

Fig. 4: (a) VSI dq inner current control (b) Inverter dq closed-loop control

III. Simulation Results and Discussion

The three-phase grid-connected PV inverter topology in Fig. 1, proposed to investigate the inverter's and IM's behavior when injecting reactive power required by the load on stabilizing the weak grid, is simulated in PSIM software using the parameters given in Table 1.

TABLE I. Simulation Parameters

AC System Parameters		**Induction Motor Parameters**	
Grid Line Voltage	415 V	Nominal Line Voltage	400 V
Frequency	50 Hz	Number of Poles	4
Grid Impedance SCR	5	Frequency	50 Hz
Grid Impedance X/R	0.3	Rotor Speed	1435 rpm
60% oversized inverter	19.2 kVA	Rated Power	5 hp
DC System Parameters		Stator Resistance	1.62 Ω
PV Power	12 kW	Stator Inductance	9.53 mH
DC Voltage	800 V	Rotor Resistance	1.62 Ω
DC link capacitor	1.5 mF	Rotor Inductance	9.53 mH
		Magnetizing Inductance	226.9 mH

The IM parameters in Table 1 are taken from [24]. A 12 kW PV array is configured for supplying DC power to the inverter on standard test conditions of irradiance and temperature. The inverter's dynamics were examined by oversizing the inverter into 60%. The 1.60 AC-DC power ratio enabled the inverter to output 19.2 kVA as the inverter's capacity with 15 kVAR reactive power. The 60% oversized inverter run in DMO and NMO with a 5hp IM started on DOL. The IM was first simulated in a strong grid and the weak grid systems without PV integration and obtained the IM's power requirement on the strong grid and the weak grid system's defective powers. Next, the PV grid inverter simulated on DMO with 60% oversized inverter capacity. Then simulated on NMO by injecting only the reactive power of the 60% capacity, and lastly simulated on NMO injecting all the IM required reactive power. The results of the simulation are presented as follows:

A. The Results on Powers Injection

The system injected active and reactive powers, as shown in Fig. 5. The MPPT accurately extracted the 12 kW DC power via boost converter from the PV array and injected it into the grid via the inverter. The extracted power is the active power supplied by controlling the DC-Link capacitor voltage, as shown in Fig. 5(a). At steady-state between 0.50 s to 0.54 s, the DC-Link voltage fluctuated within 1 % of the voltage with a ripple of about 0.5 %.

The dynamic application of reactive power injection to the weak grid is based on the load's demand to resolve voltage dip issues. The effect of IM startup on the weak grid is shown in Fig. 5(b) and Table 2. During the startup, the voltage dropped, and the system responded by injecting reactive current for the dip shown in Fig. 5(c). Before startup from 0.5 s to 0.6 s, the voltage and current are in phase, and only active power is injected into the grid. At the time of startup, 0.6 s, the voltage level reduced, the current shifted to an angle proportional to the injected reactive current for the startup's duration from 0.6 s to 0.85 s, and the current amplitude rise, which indicated the reactive power injection.

TABLE II. Grid Voltage Vip

Parameter	**Grid**[1]	**Steady State**		**Start-up**		**Loading**	
	Voltage (V)	**Voltage (V)**	**Volt. Level**	**Voltage (V)**	**Volt. Level**	**Voltage (V)**	**Volt. Level**
Strong Grid	239.6	239.6	100%	239.5	100%	239.8	100%
Weak Grid	239.6	239.5	100%	191.6	80%	224.9	94%
PV DMO[2], 60% oversized inverter.	239.6	271.5	113%	233.5	97%	261.8	109%
PV NMO[3], 60% oversized inverter.	239.6	239.5	100%	204.2	85%	227.3	95%
PV NMO[3], Inverter Fully used	239.6	239.6	100%	205.7	86%	227.3	95%

[1.] The rated grid phase voltage.
[2.] Day Mode Operation operation of PV inverter.
[3.] Night mode operation of PV inverter.

Table 2 showed the effectiveness of reactive power injection into the grid on the voltage levels. The strong grid system is taken as a reference. On no load steady-state, voltage swell occurred during the inverter's DMO. In contrast, the standard voltage level is given on the inverter's NMO operations at the steady-state. The DMO gave tolerable voltage levels for 15 kVAR injected During startup. However, the NMO startup resulted in voltage dip for both 15 kVAR injected and the average 17 kVAR IM's required reactive power injected. The voltage sag is below the accepted level of the IEC 61000-4-30 standard for the weak grid and the two NMO startups. Nevertheless, all the voltages are within the plus and minus 10% of the tolerable standard levels on loading.

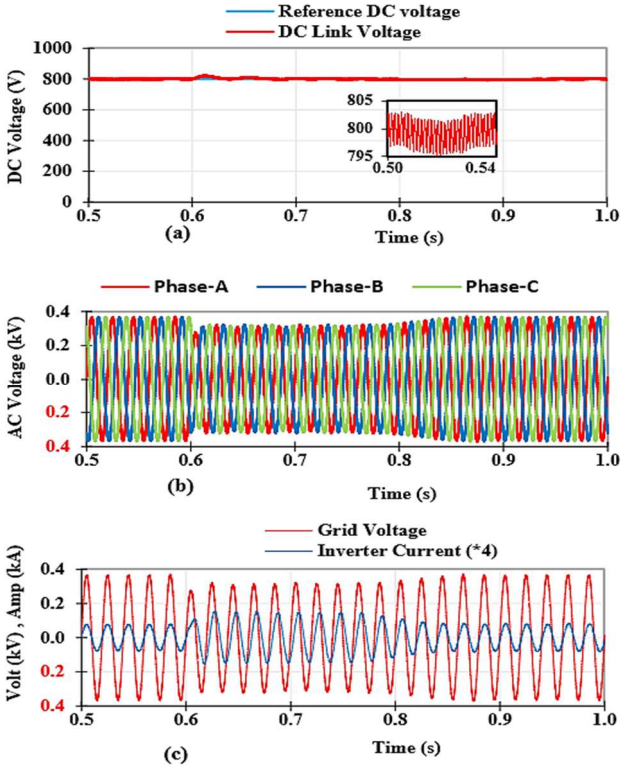

Fig. 5: (a) DC link voltage (b) Grid voltage (c) Reactive current injection

B. The Results On Inverter and IM Dynamics

The inverter's injected active and reactive powers on the weak grid PV DMO and NMO on no-load startup and loading of the IM at full load were presented in Fig. 6 and Fig. 7. In Fig. 6(a), before startup, the inverter injected the 12 kW into the grid. The IM absorbed the inverter's power and part of the grid's active power upon startup since the IM's active power demand is higher than the inverter's injected active power. As a result, the IM absorbed all the required active power from the grid on the NMO, as shown in Fig. 6(b). The 60% oversized inverter injected the 15 kVAR in Fig. 6(c), and the remaining reactive power was absorbed from the grid.

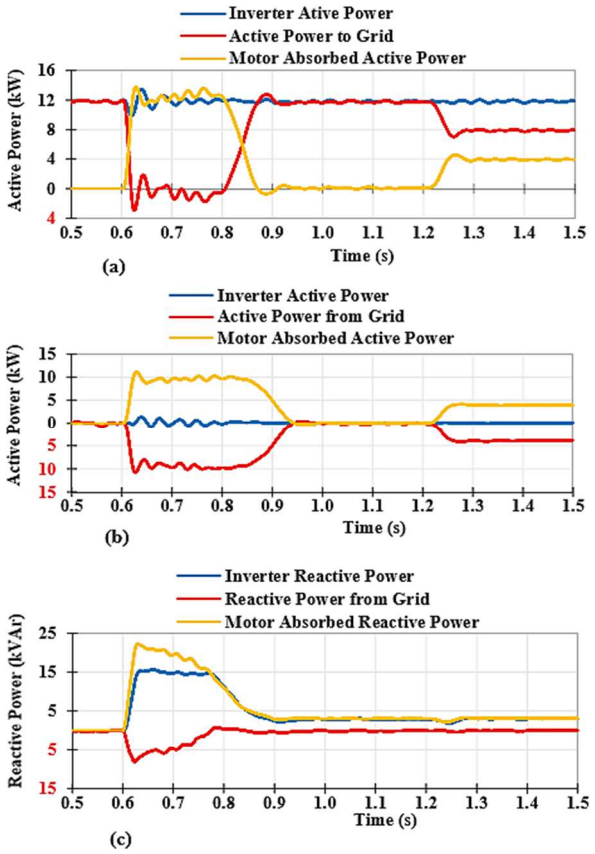

Fig. 6: (a) DMO active power (b) NMO active power (c) DMO reactive power with oversized inverter

Fig. 7 represents the results of active and reactive power absorbed by the IM during startup and loading. It shows that the IM started on a strong grid absorbed peak and average active power of about 15.5 kW and 12 kW, and reactive power of about 23.5 kVAR and 17.1 kVAR, respectively. It is also utilized on loading a peak and average active power of about 4.18 kW and 3.96 kW, and reactive power of about 2.76 kVAR and 2.73 kVAR, respectively. These values are reference values used to analyze the system. Fig. 7(a) and (b) presented the IM active and reactive power, respectively, show that the IM's power requirement on weak grid startup is not achievable to the reference values obtained.

Integrating the inverter improved both active and reactive power consumption of the IM. The IM absorbed powers efficiently, which are very closed to its standard capacity on the weak grid DMO of the inverter. However, its standard power consumption is not smoothly achieved, as seen in Fig. 7(a) and (b). The weak grid PV NMO shows a slight improvement from the weak grid IM startup power absorption. In Fig. 7(c) and (d), the IM's active and reactive powers during full-load loading were presented, respectively. The active power consumption from all the grid systems is almost met the required reference IM active power. During the weak grid PV DMO, the IM encountered high active power build-up before attaining steady-state loading due to the grid's highly active and reactive power. In Fig. 7(d), the IM absorbed excess reactive power on full-load loading during the weak grid PV DMO. This extra reactive power might cause overheating on the stator winding of the IM if it increases.

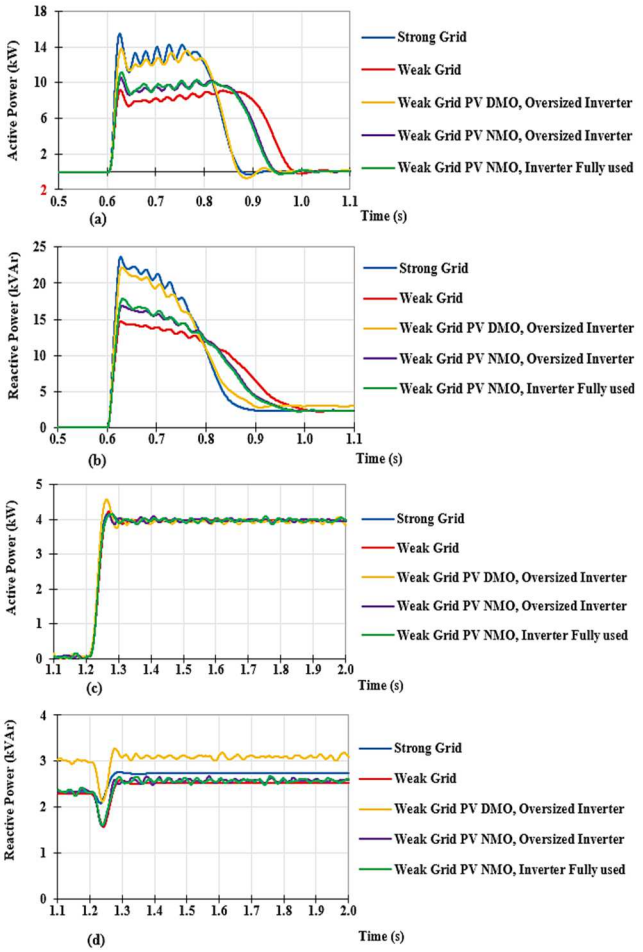

Fig. 7: (a) IM startup active power, (b) IM startup reactive power, (c) IM loading active power, (d) IM loading reactive power.

The dynamic responses of the IM's on the speed and torque during startup are shown in Fig. 8. (a) and (b), respectively. It is seen from Fig. 8(a) and (b) that the IM build-up fast speed and developed high torque during the weak grid PV DMO startup compared to the weak grid network and weak grid PV NMO startups. The improvement on the weak grid PV NMO startups is slightly showed in the speed and torque. During weak grid PV DMO startup, the breakdown torque of the IM is comparable to the strong grid startup. However, the starting torque peak on the weak grid PV DMO startup is less than the strong grid startup.

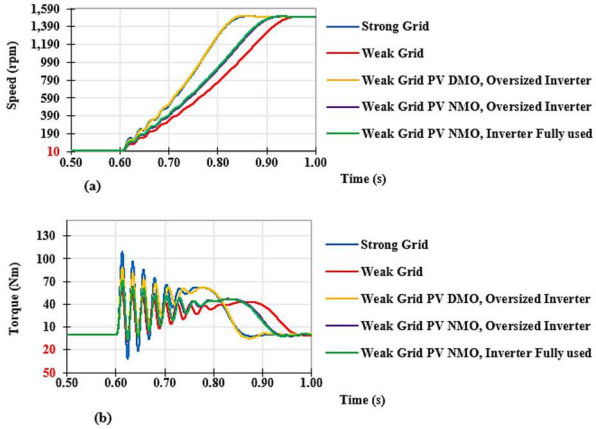

Fig. 8: (a) IM startup speed, (b) IM startup torque

IV. CONCLUSION

A three-phase grid-connected PV inverter injecting active power and the motor-required reactive power is simulated to investigate the inverter's and motor's behavior when compensated a high reactive power requested by the IM. The IM was simulated with a strong grid, weak grid, and 60% oversized PV inverter weak grid on DMO and NMO. The inverter injected 12 kW active power and 15 kVAR reactive power on DMO. It also injected 15 kVAR reactive power without fully utilized the inverter and 17 kVAR by entirely using the inverter during NMO. The results showed that the reactive power injected during DMO improved the voltage with voltage swells of 113% on steady-state, 97% on startup, and 109% on loading. On the other hand, the voltage improvement on NMO is very minimal due to the excessive reactive power injected. In all the grid conditions, the IM performance and the grid stability are superior on the inverter's DMO. However, the IM performance is not accurate as expected due to the excess reactive power injected into the grid, which justifies the need for modified IM drives for good IM performance and better grid voltage stability.

ACKNOWLEDGMENT

The authors gratefully acknowledged the Government of Indonesia and the Strategic Research Grant 2021 from the Electrical Engineering Department, Diponegoro University, for the sponsor of this work.

REFERENCES

[1] O. Gandhi, C. Rodríguez-Gallegos, T. Reindl, and D. Srinivasan, "Competitiveness of PV inverter as a reactive power compensator considering inverter lifetime reduction," *Energy Procedia*, vol. 150, pp. 74–82, 2018, doi: 10.1016/j.egypro.2018.09.005.

[2] J. F. Gómez-González *et al.*, "Reactive power management in photovoltaic installations connected to low-voltage grids to avoid active power curtailment," *Renew. Energy Power Qual. J.*, vol. 1, no. 16, pp. 5–11, 2018, doi: 10.24084/repqj16.003.

[3] S. Kocman, P. Orsag, and P. Pecinka, "Simulation of startup behaviour of induction motor with direct online connection," *Adv. Electr. Electron. Eng.*, vol. 15, no. 5, pp. 754–762, 2017, doi: 10.15598/aeee.v15i5.2342.

[4] N. Afrin, F. Yang, J. Lu, and M. Islam, "Impact of Induction Motor Load on the Dynamic Voltage Stability of Microgrid," *2018 Aust. New Zeal. Control Conf.*, pp. 397–402, 2018, doi: 10.1109/ANZCC.2018.8606599.

[5] P. Aree, "Impacts of Small and Large Induction Motors on Active and Reactive Power Requirment and System Loadability," no. I, pp. 51–54, 2014.

[6] T. Javied, T. Rackow, R. Stankalla, C. Sterk, and J. Franke, "A Study on Electric Energy Consumption of Manufacturing Companies in the German Industry with the Focus on Electric Drives," *Procedia CIRP*, vol. 41, no. December, pp. 318–322, 2016, doi: 10.1016/j.procir.2015.10.006.

[7] A. G. Yetgin, M. Turan, B. Cevher, A. İ. Çanakoğlu, and A. Gün, "Induction Motor Design Process and the Effect of Output Coefficient," no. June, 2018.

[8] A. Ilo, "Effects of the Reactive Power Injection on the Grid—The Rise of the Volt/var Interaction Chain," *Smart Grid Renew. Energy*, vol. 07, no. 07, pp. 217–232, 2016, doi: 10.4236/sgre.2016.77017.

[9] S. Saiprasad, N. Soni, and S. Doolla, "Analysis of motor starting in a weak microgrid," *2014 IEEE Int. Conf. Power Electron. Drives Energy Syst. PEDES 2014*, 2014, doi: 10.1109/PEDES.2014.7042127.

[10] A. Ali, D. Raisz, and K. Mahmoud, "Optimal oversizing of utility-owned renewable DG inverter for voltage rise prevention in MV distribution systems," *Int. J. Electr. Power Energy Syst.*, vol. 105, no. June 2018, pp. 500–513, 2019, doi: 10.1016/j.ijepes.2018.08.040.

[11] R. K. Varma, B. Das, I. Axente, and T. Vanderheide, "Optimal 24-hr utilization of a PV solar system as STATCOM (PV-STATCOM) in a distribution network," *IEEE Power Energy Soc. Gen. Meet.*, pp. 1–8, 2011, doi: 10.1109/PES.2011.6039864.

[12] M. Habyarimana and D. G. Dorrell, "Methods to Reduce the Starting Current of an Induction Motor," *2017 IEEE Int. Conf. Power, Control. Signals Instrum. Eng.*, pp. 34–38, 2017.

[13] D. Wang, Y. Shen, Z. Hu, T. Cui, and X. Yuan, "Active and reactive power joint balancing for analyzing short-term voltage instability caused by induction motor," *Energies*, vol. 12, no. 19, 2019, doi: 10.3390/en12193617.

[14] A. S. Omran, N. H. Abbasy, and R. A. Hamdy, "Enhanced performance of substation dynamics during large induction motor starting using SVC," *Alexandria Eng. J.*, vol. 57, no. 4, pp. 4059–4070, 2018, doi: 10.1016/j.aej.2018.10.009.

[15] C. C. Gomes, A. F. Cupertino, and H. A. Pereira, "Damping techniques for grid-connected voltage source converters based on LCL filter: An overview," *Renew. Sustain. Energy Rev.*, vol. 81, no. June, pp. 116–135, 2018, doi: 10.1016/j.rser.2017.07.050.

[16] N. Hamrouni, S. Younsi, and M. Jraidi, "A flexible active and reactive power control strategy of a LV grid connected PV system," *Energy Procedia*, vol. 162, pp. 325–338, 2019, doi: 10.1016/j.egypro.2019.04.034.

[17] F. Schimpf and L. E. Norum, "Grid connected Converters for Photovoltaic , State of the Art , Ideas for Improvement of Transformerless Inverters Department of Electrical Power Engineering Department of Electrical Power Engineering," *Nord. Work. Power Ind. Electron.*, 2008.

[18] T. I. Suyata, S. Po-Ngam, and C. Tarasantisuk, "The active power and reactive power control for three-phase grid-connected photovoltaic inverters," *ECTI-CON 2015 - 2015 12th Int. Conf. Electr. Eng. Comput. Telecommun. Inf. Technol.*, vol. 2, no. 1, 2015, doi: 10.1109/ECTICon.2015.7207066.

[19] I. Setiawan, M. Facta, A. Priyadi, and M. H. Purnomo, "Investigation of Symmetrical Optimum PI Controller based on Plant and Feedback Linearization in Grid- Tie Inverter Systems," vol. 7, no. 3, 2017.

[20] R. Izah, S. Subiyanto, and D. Prastiyanto, "Improvement of DSOGI PLL Synchronization Algorithm with Filter on Three-Phase Grid-connected Photovoltaic System," *J. Elektron. dan Telekomun.*, vol. 18, no. 1, p. 35, 2018, doi: 10.14203/jet.v18.35-45.

[21] M. Merai, M. W. Naouar, and I. Slama-belkhodja, "An Improved DC-Link Voltage Control Strategy for Grid Connected Converters," vol. 8993, no. c, pp. 1–8, 2017, doi: 10.1109/TPEL.2017.2707398.

[22] J. Y. Lee, Y. P. Cho, H. S. Kim, and J. H. Jung, "Design methodology of passive damped LCL filter using current controller for grid-connected three-phase voltage-source inverters," *J. Power Electron.*, vol. 18, no. 4, pp. 1178–1189, 2018, doi: 10.6113/JPE.2018.18.4.1178.

[23] R. Aparnathi and V. V. Diwedi, "Study of the LCL Filter for Three Phase inverter in higher stability for the Active damping Method using Genetic Algorithm Base .," *Int. J. Adv. Technol.*, vol. 4, no. 1, pp. 36–49, 2013.

[24] A. K. Adapa and V. John, "Active phase-converter for operation of three-phase induction motors on single-phase grid," *IEEE Int. Conf. Power Electron. Drives Energy Syst. PEDES 2016*, vol. 2016-Janua, pp. 1–6, 2017, doi: 10.1109/PEDES.2016.7914362.